

## Review of research on cars wake flow control methods to reduce aerodynamic drag

*Mohamed Maine<sup>1</sup>, Mohamed El Oumami<sup>2</sup>, Otmane Bouksour<sup>2</sup>, and Abdeslam Tizliouine<sup>2</sup>*

<sup>1</sup>PhD Student, Higher National School of Electricity and Mechanics,  
University Hassan II,  
Casablanca, Morocco

<sup>2</sup>Laboratory of Production, Mechanics and Industrial Engineering,  
Higher School of Technology, University Hassan II,  
Casablanca, Morocco

Copyright © 2019 ISSR Journals. This is an open access article distributed under the *Creative Commons Attribution License*, which permits unrestricted use, distribution, and reproduction in any medium, provided the original work is properly cited.

**ABSTRACT:** The reduction of aerodynamic drag is a primordial element to reduce the energy consumption for ground vehicles, thus reducing greenhouse gases. This paper reviews on methods of controlling the wake flow of bluff body to reduce its aerodynamic drag. The study is limited to methods that allow a significant drag reduction greater than 3%, studied on generic cars, in the last eight years (2010-2018). There are two main methods of controlling the wake flow: passive control (vortex generator, underbody device, deflector, tail plate ...) which is based on the installation of a device on the car to modify the vortices and active control (steady blowing, pulsed jets, suction, fluid oscillators...) which modifies the wake of a car by setting up an additional energy. In addition, other methods allow coupling between different techniques. There is a wide variation in the drag reduction obtained for all these methods. Some of them can be industrialized and others are limited by design and habitability constraints.

**KEYWORDS:** Aerodynamic, Drag reduction, Passive control, Active control, Generic car.

### 1 INTRODUCTION

The industrial world is today in perpetual evolution and the demand in energy continues to increase. Much of this energy is consumed by means of transportation. Energy needs are increasing in both developed and emerging countries and even in developing countries. Alongside this, there are new requirements and environmental concerns that are needed in terms of pollution reduction and compliance with environmental protection standards. These two aspects directly concern car manufacturers. This is why they are moving towards optimizing current technologies or proposing new technologies to reduce vehicle consumption and/or air pollution. For ground vehicles, the energy consumption depends on the speed of the ride. According to Eulalie, from 65 km/h, the part of the air resistance remains lower than the energy used to move the mass of the car [1]. This aerodynamic resistance increases rapidly to over 90% at high speeds [2]. The reduction of energy consumption needs the optimization of the shape of the car so that it does not oppose the aerodynamic efforts on the road.

Several parts of the vehicle contribute to aerodynamic training (mirrors, wheels, rear glasses, rear base). Hucho and Sovran [3] show that the detachment field in the rear end of the car contributes to more than 40% of aerodynamic training.

### 2 EFFECT OF AERODYNAMIC DRAG ON ENERGY CONSUMPTION

The strong global demand for fossil fuel sources and the environmental degradation caused by vehicle pollution, push driving automotive manufacturers to think of alternative sources of energy such as electric energy, with a minimum energy consumption. It has been estimated that 1% increase in fuel economy in United States, can save  $1 \times 10^6$  m<sup>3</sup> of fuel per year [4].

Drag reduction is a good solution to reduce fuel consumption. As environmental benefits, a drag reduction of 30% contributes to 10 g/km of CO<sub>2</sub> reduction [5].

Among the aspects on which we can act to reduce consumption, the aerodynamics of the car. Engineers and researchers have noted that aerodynamic forces on a car consist of pressure forces and friction forces. It has shown that the pressure forces represent 80%, whereas the friction forces represent only 20% [6]. Therefore, to reduce the aerodynamic drag it is necessary to act most on the pressure forces.

### 3 AHMED BODY MODEL

A real-life automobile is very complex shape to model or to study. However, (Ahmed et al. 1984) proposed a simplified model of ground vehicle to investigate the three-dimensional regions of separated flow, which may enable a better understanding of such flows. The geometry of Ahmed's body is as follows (Fig. 1): L=1044 mm; W=389 mm; h=288 mm; the oblique part is 222 mm long and the lower surface of Ahmed's body is 50 mm above the ground.

The angle of the rear inclined surface strongly influences the flow around this body, which indicates that much of the aerodynamic drag is generated by the development of the three-dimensional separation of the vortices of the rear inclined surface [7]. It was found also that the drag coefficient of the Ahmed's body increases with the yaw angle [8], [9], [10]. Several authors have used Ahmed's body as a reference for studying the aerodynamics of ground vehicles.

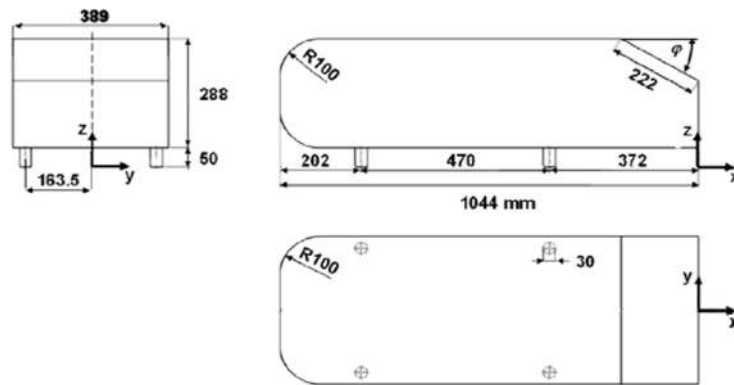


Fig. 1. Ahmed Body geometry [11]

### 4 AERODYNAMIC DRAG REDUCTION METHODS

To reduce the aerodynamic drag of vehicles, there are several methods, namely shape optimization, but that remains limited by design constraints and habitability. Researchers have developed other techniques that allows the modification of the flow around a volume. These techniques are mainly divided into two categories: active and passive control methods. The active technique uses additional energy produced by actuators requiring power generally taken from the main energy generator of the vehicle. The investigation concerning the active flow control devices was presented by using different techniques: synthetic jets [12], pulsed jets [13], [14], [15], [16], [17], suction [18], [19], blowing [20], [21], [22], [23] and fluid oscillators [24].

The passive flow control method consist on the use of discrete obstacles, added around or on the roof of the vehicle. This method include the use of several techniques: vertical splitter plates [25]. Flaps [26], [27], [28]. Vortex generators [29], [30], [31], [32], [33]. Rounded top edge of the slanted surface [34]. Deflectors [35], [36], [5], [37]. Non-smooth surface [38]. Rear screen & rear fairing [31]. Underbody devices [39]. Streaks [40]. Jet Boat Tail [41]. Base cavity [42], [43]. Lateral guide vane [44]. Underbody diffuser [45], [46], [47], [48]. Porous layer [49] and tail plate [50].

There are also several coupled control techniques to reduce the drag coefficient: blowing jets, pulsed jets and porous layers [51]. Tapering and blowing [52]. Blowing and suction [53], [54]. Steady blowing with a base cavity [55] and tapering & blowing into the base [52].

The passive methods are better than the active ones [27]. The merits of these approaches are that they require no energy expenditure, no input from the user and are cheaper than active techniques. It is interesting to mention that there are others

general techniques used to decrease the drag for ground vehicles as the following car for cyclist [2], the cab-roof fairings for heavy vehicles [56], the bobsleigh model [57] and others. Among these flow control methods developed by researchers, there are those already marketed, while others are still in the process of improvement.

In this paper, we will limit our study to research that satisfies three conditions: articles published in last eight years (between 2010 and 2018), and investigations allowing a significant drag reduction greater than 3%, tested on generic cars (With body type's hatchback, Sedan and SUV) (Fig.2).

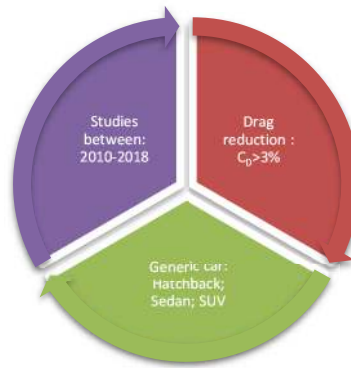


**Fig. 2. Limits of this review**

## 5 PASSIVE CONTROL METHODS

Passive control method consists of modifying the flow around ground vehicle by adding devices in specific places. They can be declined in two groups according to their influence on the flow control. In the first group, the obstacles are positioned on the surface of the geometry while in the second they are upstream or downstream of the geometry to be controlled [4].

### 5.1 VERTICAL SPLITTER PLATES (VSP)

(Gilliéron and Kourta, 2010) investigated the role of vertical splitter plates (VSP) placed on a simplified geometry MPV type vehicle, represented by Ahmed body, at scale 0.75, Fig.3. Experimental study was taking in Prandtl-type closed wind tunnel for Reynolds numbers between  $Re=1.0 \times 10^6$  and  $Re=1.6 \times 10^6$ . Drag reduction about 28% were observed for the VSP angle  $\theta=0^\circ$ . These results can be industrialized to reduce car aerodynamic drag and thus reduce energy consumption [25].

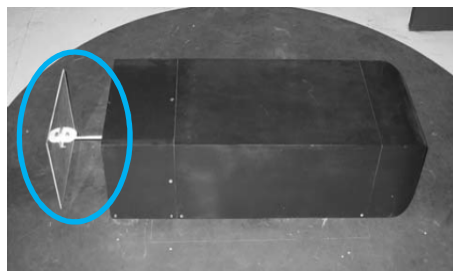


**Fig. 3. Ahmed's body model with vertical splitter plates [25]**

### 5.2 VORTEX GENERATORS

Vortex Generators (VG) are a small dispositive that change the vortex forms (Fig.4). These devices are widely used to control the boundary layers for higher speeds. Several studies have been conducted on VGs in recent years, but have not achieved to significant reductions in aerodynamic drag. Among these searches (Kim and Chen, 2010) made test on Low Mass Vehicle of a minivan, and obtain 2.8% of drag reduction [30]. (Rohatgi, 2012) tested VGs on a small model of General Motors, with 1.24% drag reduction [31].

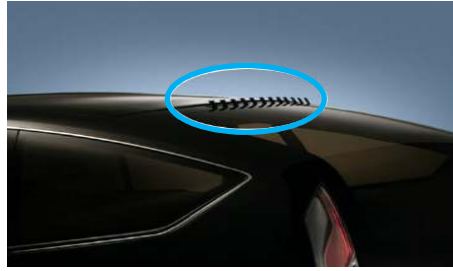


**Fig. 4. VGs installed on the edge of generic car [31]**

In addition, (Dubey et al., 2013) made VGs tests on two models of cars: Sedan (-0.9%) and Hatchback (-0.8%) [32]. The most important research of VGs was done by (Arya et al., 2017) who studied a model of passenger car with add-on-devices [33]. The model was created by CATIA software, and analyzed by CFD ANSYS CFX. The percentage drop of drag force and lift force are respectively 8.7% and 12.8%. This was obtained by attaching VGs & spoiler on the same car.

### 5.3 DEFLECTORS

(Fourrié et al., 2011) studied experimentally in a supersonic wind tunnel of (TEMPO) laboratory at the University of Valenciennes the reduction of aerodynamic drag on a generic vehicle. The model used is a deflector installed on Ahmed body with a 25° rear slant angle. The inlet velocity is between  $U_0=16$  and 40 m/s for Reynolds numbers between  $Re=3.1 \times 10^5$  and  $7.7 \times 10^5$ . The use of deflector increases the separate region on the rear window. The widening of this flow region disturbs the development of longitudinal vortices rotating in opposite directions on the lateral edges of the rear window. This phenomenon leads to a drag reduction of up to 9% depending on the deflector angle [35].

(Hanfeng et al., 2015) investigate the effects of deflectors on the aerodynamic drag and near wake of an Ahmed model with a 25° slant angle (Fig.5). Experiments were conducted in a closed circuit low speed wind tunnel at a Reynolds number of  $Re=8.7 \times 10^5$ , for inlet velocity  $U_0=25$  m/s. The deflectors were placed at the side edges and leading edge of the slant of Ahmed body model. The deflector at the leading edge of slant changes the near wake of the model similar to that behind an Ahmed model of 35° slant angle, eliminating the D-shape separation bubble on the slant. The corresponding drag reduction observed were respectively 9.3%, 10.7% and 10.9% for the deflector width of 1%, 2% and 3% of  $l$ . For the 25° slant Ahmed model, the deflector placed at the leading edge of the slant is more efficient in reducing drag and suppressing the trailing vortices than those at the side edges of slant [59].

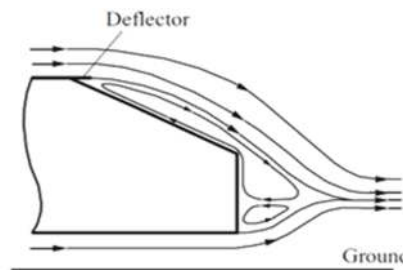


**Fig. 5. Ahmed Body with top-edge-mounted deflector [59]**

(Raina et al., 2017) tested the deflector installed on Ahmed body for reducing aerodynamic drag. The CFD GAMBIT & Fluent with k- $\epsilon$  SST (Shear Stress Transport) model are used in this study. The deflector angles are varied from -25° to 60° at two inlet flow velocities of  $U_0=16$  m/s and  $U_0=40$  m/s. The results obtained have a drag reduction of nearly 7% [36].

### 5.4 NON-SMOOTH SURFACE

It's a method that applies the principle of the golf ball's shape on the outer surface of the car (Fig.6). It makes the surface in contact with the air a dimpled non-smooth surface in order to allow the absorption of the vortices generated on the boundary layer.

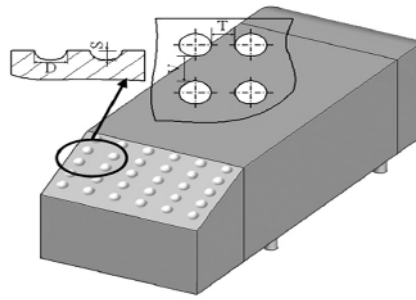


**Fig. 6. Ahmed's body with non-smooth surface [38]**

This principle can be divided into two types. One is to promote a turbulent boundary layer, leading to delayed flow separation, thereby obtaining a smaller wake. The other is primarily to reduce the skin friction.

(Yiping et al., 2016) conducted a numerical study of the effect of the non-smooth surface installed on the back sloping surface of Ahmed's body. The use of a Kriging surrogate model to search an optimal design has reduced the aerodynamic drag coefficient by 5.20% [38].

### 5.5 REAR SCREEN AND REAR FAIRING

(Rohatgi, 2012) tested the aerodynamic drag reduction on a small model of a General Motor SUV (L=1710 mm) in wind tunnel TAD-2 of the National Aviation University of Ukraine (NAU) [31]. Two passive methods were used. The first is a rear screen: an extended plate at the rear of the car (Fig.7).



**Fig. 7. SUV model with rear screen [31]**

The second is a rear fairing: an aerodynamic extension of the rear of the car (Fig.8). Aerodynamic reductions observed are, 6.5% for the first device, and 26% for the second. These drag reductions are obtained in relation to the constraints of aesthetics and habitability.



**Fig. 8. SUV model with rear fairing [31]**

### 5.6 STREAKS

(Pujals et al., 2010) got an aerodynamic drag reduction of 10% by using cylindrical roughness: elements installed on the back of Ahmed's body with a 25° rear slant angle (Fig.9) which allow the modification of the recirculation flows located on the back layer. The experimental study was done in PSA wind tunnel type Eiffel for inlet velocity  $U_0=5$  up to 55 m/s and Reynolds number  $Re = 1.35 \times 10^6$  [40].

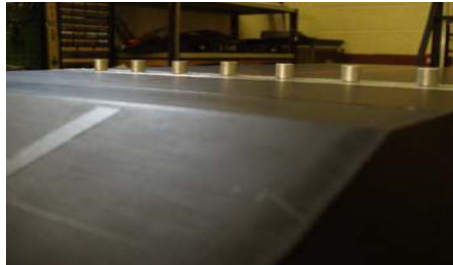


*Fig. 9. Ahmed's body model with streaks [40]*

### 5.7 TAIL PLATES

(Sharma and Bansal, 2013) published a research about a model of a passenger car with tail plates that reduces aerodynamic drag to 3.87% and 16.62% lift coefficient [50]. The Sharma's model was digitally created by Solidworks 10, and simulated on CFD software ANSYS 14.0 Fluent, using k- $\epsilon$  steady model of turbulence. The tail plates are placed at backside of the roof and at the tail bumper of the passenger car at 12° inclination angle. The arrangement of them is shows in Fig.10.

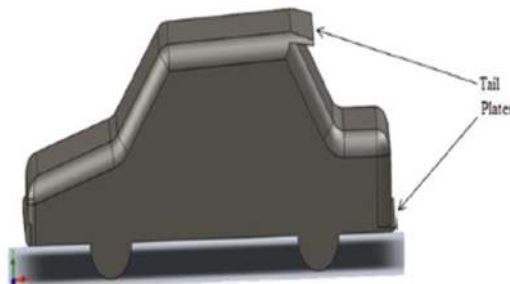


*Fig. 10. Sharma's model with tail plates [50]*

### 5.8 LATERAL GUIDE VANES (LGV)

LGV are devices installed near the rear end of the vehicle to channel airflow from the wake area to improve pressure recovery.

(Wahba et al., 2012) studied LGV on a simplified model of SUV (Fig.11) to decrease aerodynamic drag. Numerical tests were done by CFD ANSYS CFX with RANS equations and two turbulence models (k- $\epsilon$ ; SST k- $\omega$ ) for an inlet velocity  $U_0=120$  km/h at 25°C. This method with symmetric airfoils, such as NACA 0015, reduces the drag by 18% [44].

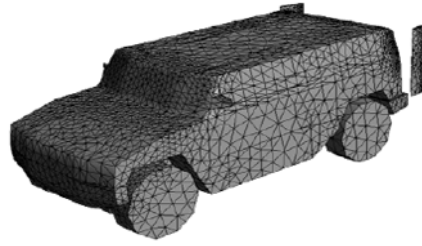


Fig. 11. SUV model with LGV [44]

5.9 UNDERBODY DEVICES

(Junho et al., 2017) presents research on the use of the underbody devices (undercover, under-fin, and side air dam) at the bottom of a sedan car (Fig.12). The model chosen is YF-Sonata from Hyundai Motor Company (HMC). The results were evaluated by CFD Fluent with k-ε steady model, for the inlet flow velocity of  $U_0=120$  km/h. The drag reduction observed was 8.4% [39].

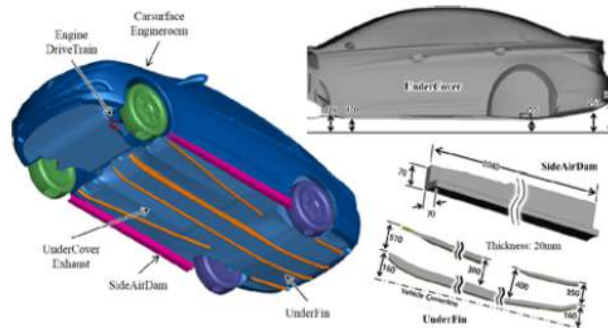


Fig. 12. YF-Sonata model with underbody devices [39]

5.10 UNDERBODY DIFFUSER

(Kang et al., 2012) tested underbody diffuser device on a model of passenger car (type notchback, Fig.13) to decrease aerodynamic drag. The model of passenger car was created by VMF (Vehicle Modeling Function) and simulated on CFD ANSYS Fluent with different equations (DES; LES; RANS), for  $U_0=70$  km/h~160 km/h. Six cases of diffuser devices with different lengths were tested. Among the various lengths of the diffuser, case 6 (length 450 mm) showed the best drag reduction performance, with an average reduction of more than 4% [45].

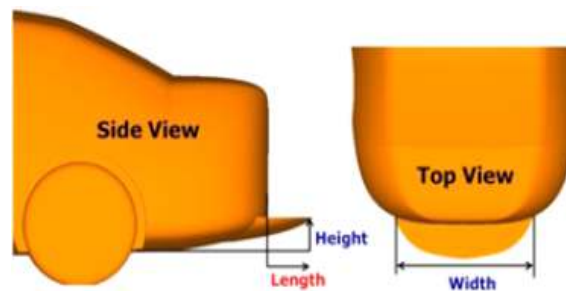


Fig. 13. Model of notchback car with underbody diffuser [45]

Also, (Marklund et al., 2013) studied the role of an under-body diffuser. Two car models were tested: Saab 9-3 Sedan and Wagon of 2012 model year. The experimental tests and measurements were carried in the Saab Climatic wind tunnel at a range of vehicle speeds from  $U_0=40$  to 200 km/h. The numerical simulation was completed in CFD Fluent 14.0, with RANS equations

and k-ε turbulent model. The optimum drag occurred at approximately 8° diffuser angle for the sedan and approximately 5° for the wagon. An increased diffuser angle reduced the lift force linearly. The reduction aerodynamic drag observed for the Sedan car was approximately 10%, and 2–3% for Wagon car [46].

(Mazyan, 2013) tested the effect of the diffusers for two models of passenger car. The first was Ahmed body in which rear wing modeled by NACA 0015 was attached at 10° from the rear slant angle. The second is an SUV represented by a Hummer model with the wing angle  $\theta = 10^\circ$  with the vertical plane. In the numerical study, both methods RANS and LES with three turbulent models (SST; RNG; k-ε) were used to calculate the rate of the aerodynamic drag reduction. The obtained results were -10% for Ahmed body and -4.2% for the Hummer model of drag reduction [47].

(Huminc and Huminc, 2017) presents results of a study of a 1:4 Ahmed body with a 35° tilted top surface at the rear, an underbody diffuser, wheels and wheelhouses. The model was generated by CAD and simulated in CFX finite volume CFD code. The diffuser length  $l_d$  and the angle  $\alpha_d$  were systematically varied. Favorable cases studied were for the following diffuser parameters:  $\alpha_d = 5^\circ$  with  $(l_d/l) = 0.2$ , and  $\alpha_d = 3^\circ$  with  $(l_d/l) = 0.4$ , where  $l$  is the car length. These cases correspond to a value of  $(h_d)$  close to 40% of the ride height ( $h$ ), in which  $h_d$  was the diffuser height. The average drag and lift increment due to the addition of wheels were respectively 5.8% and 2.43%. The study also reveals that a relatively short diffuser hasn't a relevant aerodynamic benefit for a bluff body on wheels [48].

### 5.11 JET BOAT TAIL (JBT)

(Hirst et al., 2015) used the Jet Boat Tail method to reduce aerodynamic drag of a rectangular prism bluff body similar to a small model of SUV. The jet boat tail for bluff bodies operates by surrounding a converging duct around the end of the bluff body where the base surface is located. The duct captures free stream and forms a high-speed jet angled toward the center of the bluff body base surface circumferentially to have the effect of a boat tail (Fig.14). This method makes it possible to reduce the turbulent fluctuation of the wake zone and to reduce the recirculation speed. An experimental study was conducted in University of Miami Wind Tunnel Research facility equipped by PIV (Particle Image Velocimetry). The experimental study is performed for  $U_o = 10$  m/s and 3 m/s for  $Re = 2.56 \times 10^5$ . A numerical simulation in CFD LES model was used to evaluate higher Reynolds numbers. A drag reduction of 15% was observed [41].

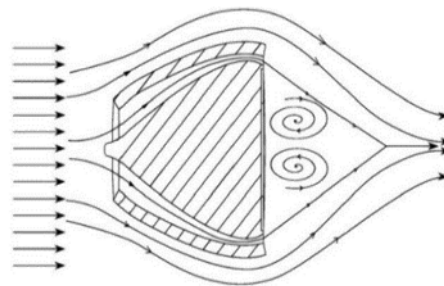


Fig. 14. Flow structure with the JBT effect influence [41]

## 6 ACTIVE CONTROL METHODS

Active control methods consists of changing shape of the vortices in the wake zone, by adding additional energy using an instrument installed in a specific place on the car body without altering the constraints of design and livability. The device used in active control is an actuator that requires an electrical energy of operation. The dissipated electrical energy for the active control must be the smallest possible compared to the energy gain due to the reduction of the aerodynamic drag by using this active control agent. For this reason, the dimensions and weight of active devices must be minimal.

Active control methods are widely used in aeronautics, and they are increasingly integrating the automotive world. There is two main techniques families': injection and blowing.

### 6.1 SYNTHETIC JETS

The operation of the synthetic jets is based on the method of the principle of alternating aspiration and blowing. Synthetic jets are useful for controlling boundary layer delimitation on profiled shapes.

(Kourta and Leclerc, 2013) studied the technique of synthetic jet on an Ahmed body scaled at 0.7 with a 25° angled rear base. Synthetic jet actuator (Fig.15) was developed by using electromechanical analogy with the help of the LEM (Lumped Element Modelling). An experimental analyze was taken in a closed-loop wind tunnel located at the PRISME laboratory, University of Orleans. Static pressure measurements, wall visualization and PIV were used to visualize flow around model. Reduction in the aerodynamic drag observed depends on the Reynolds number and the position of the actuator. This value is equal to 8.5% for  $Re=1.2 \times 10^6$  and 6.5% for  $Re=1.9 \times 10^6$ . The better control is obtained when the actuator is placed at 2 mm before the top of the rear window. The synthetic jet actuators require energy for their operations. The amount of energy required can be calculated given the parameters of the actuator (amplitude, frequency, and width) and their number. It has been found in a large number of applications that the amount of energy required is a very small fraction (< 5%) of the amount of energy saved [12].

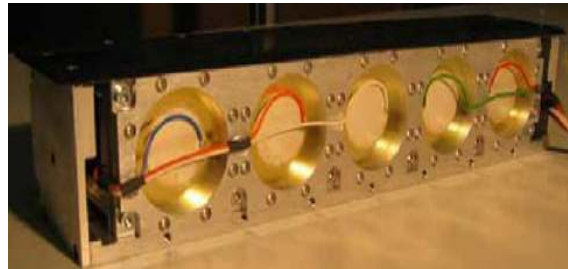


*Fig. 15. Synthetic jet actuator [12]*

## 6.2 STEADY BLOWING MICROJETS

Steady blowing microjets consist of an array of jet orifices with diameters well below the length scales of the wake or model. They are used as flow control devices that generate strong counter-rotating stream wise vortices with small energy input.

(Wassen and Thiele, 2010) investigate steady blowing through small slits near the edges of the rear surface of a model of square-back car. Numerical studies were carried out at Reynolds numbers  $Re=5 \times 10^5$  using Large Eddy Simulation (LES). The tests are realized with the SGI Attix supercomputer at the North German Cooperation for High-Performance Computing (HLRN). Many parameters are tested (change of angle between 0° and 60°, and speed flow between  $V_{\text{blow}}=0.5U_0$  and  $V_{\text{blow}}=2.5U_0$ ). The study shows that the 45° blow angle for  $V_{\text{blow}}=1.25U_0$  can maximize the aerodynamic drag reduction up to 11.1% [20].

(Aubrun et al., 2011) studied the effectiveness of blowing steady microjets technique to reduce aerodynamic drag of ground vehicle. The Ahmed body with a 25° slant (Fig.16) was presented as a model of generic car. The model was equipped with an array of blowing steady microjets 6 mm downstream of the separation line between the roof and the slanted rear window to eliminate the 3D closed separation bubble located on the slanted surface [21].

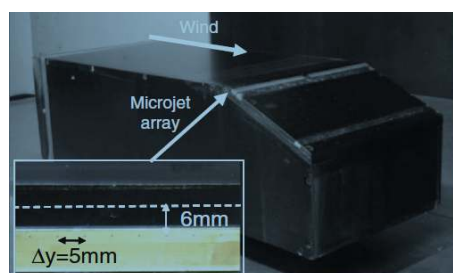


*Fig. 16. Ahmed body model with microjets [21]*

The experimental analyze was taken in the 'Lucien Malavard' wind tunnel of the PRISME Institute, University of Orleans. PIV, wall pressure and skin friction visualizations aerodynamic load measurements were used to examine changes in the flow field for  $U_0=40$  m/s at  $Re=1.95 \times 10^6$  when the control is manipulated. With the flow control by steady microjet array, a drag coefficient was reduced by 9-14% and the lift coefficient up to 42%.

(Harinaldi et al., 2013) studied the active flow control of blowing using the Ahmed body model reversed and modified (Van model). The research was carried out by two approaches namely computational and experimental methods for upstream velocity between  $U_0=13.9$  m/s and 19.44 m/s and blowing velocity  $U_b= 0.5$  m/s at Reynolds number  $Re = 2.48 \times 10^5$ . The computational approach explore Finite Volume Method (FVM), that used GAMBIT 2.4 as grid generator, for number of generated meshes volume more than 1.7 million, and the commercial solver Fluent 6.3 with k- $\epsilon$  standard turbulence model. The experimental study was taken in a wind tunnel in order to validate the aerodynamic drag reduction obtained by the computational approach. From the observed results, the blowing method gives an influence on characteristics of the flow field. The aerodynamic drag reduction obtained was 13.92% for computational study and 11.11% for experimental study. This result indicates that the blowing technique is able to reduce the wake that occurred in the back of the van model [22].

(Heinemann et al., 2014) made an experimental study on a model of car scaled 1:4 by using a fixed blow on the rear of the vehicle which aims to change the shape of the vortices that are created in the wake area. The studies are carried out in wind tunnels of the Friedrich Alexander University in Erlangen-Nuremberg (FAU) and the Technische Universitat Munchen (TUM) for flow velocity about  $U_0=30$  m/s and Reynolds number of  $Re = 2.1 \times 10^6$ . The visualization of the flows around the vehicle was carried out by LDA (Laser Doppler Anemometry), surface pressure measurements, and surface oil flow visualization. The flow field was found to be dominated by two longitudinal vortices, developing at the detachment of the rear position (C-Pillar), and a recirculating, transverse vortex above the rear window; with an air jet emerging from a slot across the surface right below the rear window section, tangentially directed upstream toward the roof section. This control method allows an aerodynamic drag reduction of 5% [23].

(McNally et al., 2015) published an article that studied the use of steady blowing micro jets as an active flow control to reduce the aerodynamic drag of ground vehicles. The model studied is a Honda Simplified Body (HSB): a flat-back ground vehicle model with rounded front and rear edges. Both experimental and numerical investigations were used. The first was taking in the FCAA Plow speed wind tunnel for a free stream velocity of 28 m/s. The second by a solver CharLES from Cascade Technologies Inc with Large Eddy Simulation Model for a free stream velocity of 14 m/s and Reynolds number of  $Re=4.8 \times 10^5$ . The use of small scale, steady micro jets in normal and tangential injection orientation is investigated. Parameters such as injection location relative to separation point, jet diameter, and blowing ratio are used. The computational approach introduces the actuator array on the top surface of the body model to support the experimental study that examines the effectiveness of flow control with micro jets installed on multiple side surfaces. The most effective at reducing drag for the considered experimental studies was the actuation at  $x/L=91.9\%$ . The wake can be modified with micro jets such that the drag experienced by the HSB is reduced by nearly 3% with also a net reduction in power consumption [60].

### 6.3 FLUID OSCILLATORS

Fluidic oscillator is a simple device containing no moving parts and that converts a steady flow input into a sweeping jet output.

(Metka and Gregory, 2015) studied a 25-deg Ahmed generic vehicle model with quasi-steady blowing at the roof–slant interface using a spanwise array of fluidic oscillators (Fig.17). The goal of this study was to reduce drag by eliminating the separation bubble on the rear slant, which is known to result in a large pressure deficit and significant total pressure losses. An experimental test was taking in the 3feet×5feet subsonic wind tunnel at the Ohio State Aerospace Research Center. Particle image velocimetry (PIV) and pressure taps were used to characterize the flow structure changes behind the model for Reynolds number near  $Re=1.4 \times 10^6$ . Oil flow visualization was used to understand the mechanism behind oscillator effectiveness. Aerodynamic drag reduction near 7% was attributed to separation control on the rear slant surface [24].

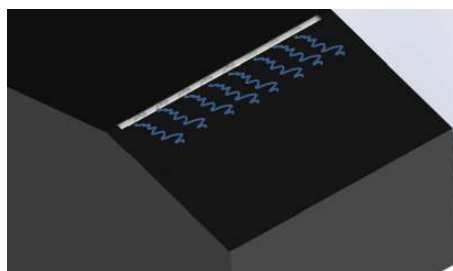


**Fig. 17. Ahmed body model with Actuators implementation [24]**

### 6.4 SUCTION

(Harinaldi et al., 2012) tested the flow over a van model (Ahmed Body scale 1:4 for 35° angle of the back, modified/reversed) using suction method (Fig.18). Both numerical and experimental investigations were tested. The suction velocity=1 m/s and upstream velocity=13.9 m/s [18].

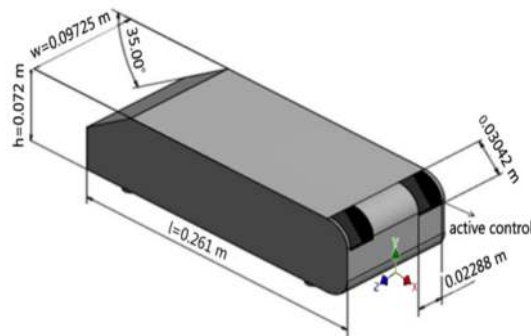


Fig. 18. Van model (Ahmed body modified/reversed) [18]

An increase of minimum value of pressure coefficient close to 26.17% and a decrease of turbulence intensity for about 12.35% are obtained by introducing suction. In the computational approach, the drag reduction have been obtained by introducing a suction for about 13.86%, meanwhile in the experimental approach, the drag reduction have been obtained for about 16.32%.

(Ait Moussa et al., 2014) introduce a methodology to identify parameters for maximum reduction of aerodynamic drag. The technique combines automatic modeling of the suction slit, computational fluid dynamics (CFD) and a global search method using orthogonal arrays. The implementation of this technique on (SUV) sport utility vehicles (Fig.19) requires adequate choice of the size and the location of the opening as well as the magnitude of the boundary suction velocity. It is shown that a properly designed suction mechanism can reduce drag by up to 9% [19].

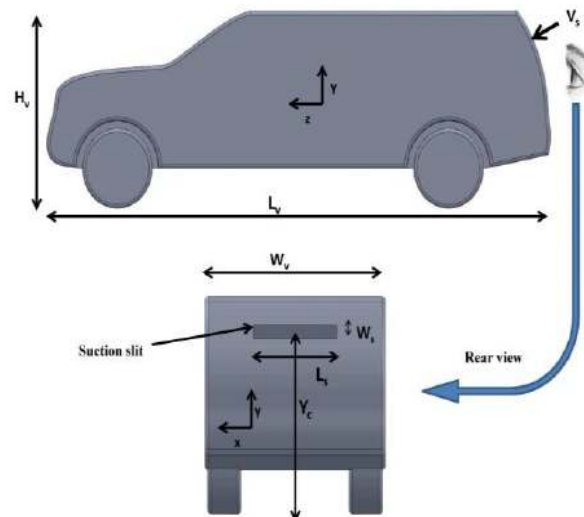
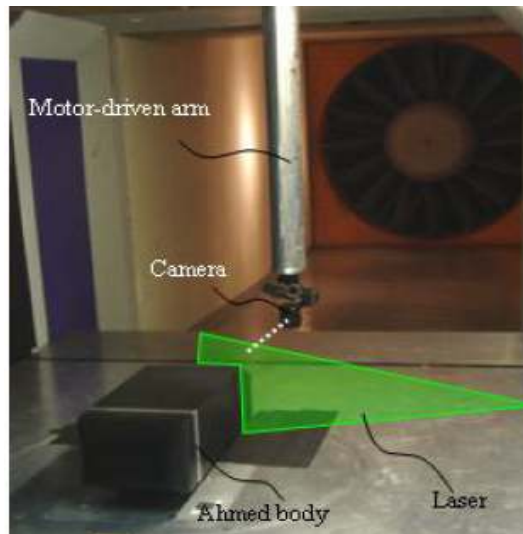


Fig. 19. SUV model with rear suction [19]

### 6.5 TRIP OF PULSED JETS

(Bideaux et al., 2011) experimentally investigate the control of flow separation on rear window of a generic vehicle shape (Ahmed body with a scale of 0.7 and a slant angle of 35°). Studies were taken in Malavard subsonic wind tunnel of the PRISME

Institute in Orleans. The model is equipped at the end of the roof with a strip of pulsed jets in order to control the flow with a velocity of 30 m/s (Fig.20) [13].



**Fig. 20. Ahmed body model tested in a wind tunnel by measurements in the median transverse plan [13]**

Drag reduction obtained was about 20% at a pulsed frequency of 500 Hz and a momentum coefficient  $C_{\mu} = 2.75 \times 10^{-3}$ . This result confirms the interest in using pulsed jets in order to reduce aerodynamic drag and pollutant emission.

(Joseph et al., 2013) published research focused on an experimental investigation of flow control of the wake tested on a 3D bluff body using Micro-Electro Mechanical System (MEMS) pulsed microjets (Fig.21). Experimental investigation was taken in the S4 full-scale automotive wind tunnel at the Institute of Aerotechnics (IAT). Significant drag reduction (>10%) was obtained at the  $Re=1.4 \times 10^6$  with micro-jets located upstream the recirculation bubble created over the rear slant of the model. The energy obtained with MEMS was better than the one obtained with conventional magnetic valves. The MEMS will be an attractive technology for future industrial vehicles applications on flow control [14].

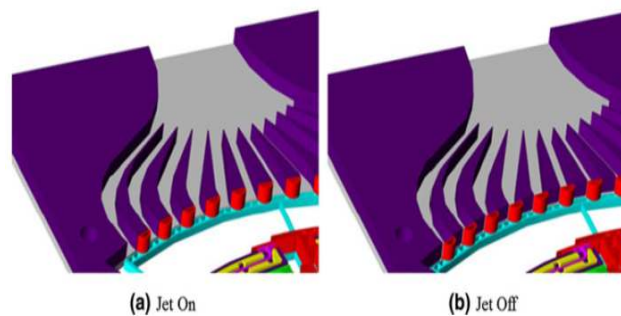


**Fig. 21. Micro-Electro Mechanical System (MEMS) pulsed microjets [14]**

(Barros et al., 2014) made an experimental study using pulsed jets. They investigated the capability of periodic pulsed jets to modify the rear pressure distribution of a three-dimensional blunt body (square-back Ahmed model) for a Reynolds number of  $Re=3 \times 10^5$ . The rear pressure variation is accompanied by large changes of the velocity field in the wake (Fig.22). Two forcing frequencies were studied and their effects on the wake were detailed. For the lower actuation frequency, a decrease of rear pressure is achieved inducing increase of the total drag of the model. The time-averaged recirculating region is shorter than the reference base flow [15].

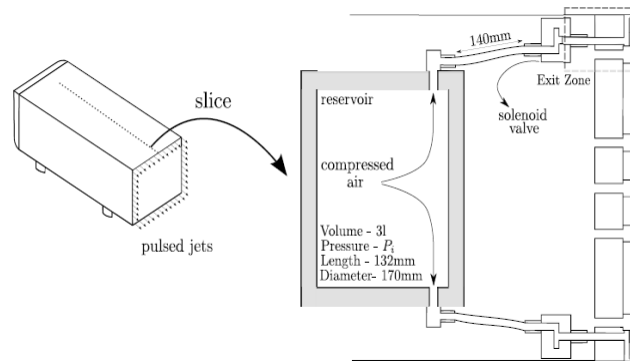


Fig. 22. Pulsed jets system [15]

The presence of strong vortex roll-up in the lower shear layer was identified which provides evidence of entrainment increase in the wake which reduces its recirculation length. Pressure gradients on the rear surface showed the inhibition of the bimodal behavior recently reported in the literature. When the actuation frequency is higher, a significant recovery of the model's base pressure was obtained, in which the pressure drag reduces by 10% and the estimated total drag reduction is about 7%. This actuated flow presents damped velocity fluctuations on the lower part of the wake (lower shear layer) and indicates a narrower and more symmetric time-averaged wake. Deviation of the mean separating streamlines was additionally noted.

(Barros et al., 2016) investigate the effect of fluidic actuation on the wake of a three-dimensional blunt body. The experimental approach was taking in a subsonic wind tunnel. The inlet velocity  $U_0$  varies between 10 m/s and 20 m/s, for Reynolds number  $Re=3 \times 10^5$ . Two flow regimes were tested: the case of broadband actuation with frequencies comprising the natural wake time scale, and the high actuation frequencies. It additionally lowers its turbulent kinetic energy thus reducing the entrainment of momentum towards the recirculating flow. By adding curved surfaces to deviate the jets by the Coanda effect, periodic actuation is reinforced. The drag reduction observed was about 20%. The unsteady Coanda blowing not only intensifies the flow deviation and the base pressure recovery but also preserves the unsteady high-frequency forcing effect on the turbulent field. This method encourages further development of fluidic control to improve the aerodynamics of road vehicles and provide a complementary insight into the relation between wake dynamics and drag [16].

## 6.6 PLASMA ACTUATOR

(Shadmani et al, 2018) conducted an experimental study using the plasma actuator. This system is composed of two electrodes separated by a dielectric barrier, whereby air molecules above the insulated electrode is ionized by establishing a strong electric field. The model used is Ahmed body with the rear slant angle of  $25^\circ$ . Experiments were performed in the open circuit wind tunnel at K. N. Toosi University (Iran). Results indicate that steady actuations at inlet velocity  $U_0=10$  m/s for Reynolds number  $Re=4.5 \times 10^5$ , the plasma actuator located on the middle of rear slant surface is capable of suppressing the flow separated from the leading edge of rear slant and sticking it back to the surface by actuating the shear layer. Aerodynamic drag reduction near 3.65% was observed [61].

## 7 COUPLING FLOW CONTROL METHODS

In order to double the gain in terms of drag reduction, several studies have been developed that allow coupling between active and passive controls.

(Bruneau et al., 2010) tested the coupling of three actions methods: blowing jets, pulsed jets and porous layers. This method was tested numerically on the Ahmed body with a  $25^\circ$  rear window model, for Reynolds number  $Re=0.3 \times 10^5$ . A Cartesian grids method is used to simulate the flow. The porous layers give the best drag reduction among the three methods and a coupling of the three actions allows reaching a 31% reduction of the drag coefficient [51].

(Jahanmiri and Abbaspour, 2011) investigate the effect of suction and base bleeding as two active flow control methods on aerodynamic drag reduction. Experimental study was taken in a subsonic closed circuit wind tunnel, for Reynolds number  $Re=2.8 \times 10^6$ . The model used was Ahmed body with  $35^\circ$  rear slant. In order to reduce the speed of the particles that make up the vortices created in the wake zone of the car, a suction in the boundary layer is applied and the sucked air was blown in the wake of the model to increase the static pressure in the wake region. The suction device was installed at the beginning of the

rear inclined surface and the blowing location was in the middle of the vertical rear part of the model. The effect of change in control flow rate, suction, and base bleeding area was investigated. Strong suction leads to drag reduction and when suction was accompanied by base, bleeding more drag reduction can be achieved. Furthermore, for a constant control flow rate, smaller suction area (control flow rates  $> 0.0035 \text{ m}^3/\text{s}$ ) and bigger base bleeding area, the reduction in drag is about 29.5% [54].

(Harinaldi et al., 2011) tested an active flow control to reduce the aerodynamic drag. The Ahmed Body scaled 1:4 for  $35^\circ$  angle of the back was used as a Van model of car. This model is equipped on the rear side with a system of blowing and suction in order to modify the near wall flow. Numerical simulation was taken by commercial solver CFD Fluent 6.3 with k- $\epsilon$  flow turbulence model. The maximum drag reduction associated with these modifications is close to 15.83% and the increase of suction velocity at  $U_{sc} > 0.3U_0$  does not improve such a reduction significantly. The drag reduction decrease when the suction velocity diminishes below  $0.3U_0$ . In an other hand, in case of blowing in rear side on reversed Ahmed body, the drag reduction is close to 14.38% and the increase of blowing velocity at  $U_b > 0.06U_0$  does not improve such a reduction significantly. Moreover, the drag reduction decrease when the blowing velocity diminishes below  $0.06U_0$  [53].

(Khalighi et al., 2012) investigated the aerodynamic drag on four different configurations, namely the baseline model (square-back, SB1), square-back with a base cavity (SB2), square-back with a boat-tail (SB3), and an active device (Coanda jet). The corresponding experiments were carried out in the wind tunnel geometry (GM R&D Basic Research Wind Tunnel) at various free-stream velocities (25 to 50 m/s). The simulations were based on unsteady RANS in conjunction with the v2-f turbulence model to study the qualitative and quantitative characteristics of the aerodynamic flow and the differences between the various configurations both in terms of global drag coefficients and in terms of the wake dynamics. The drag reductions obtained were from 18% to 50% [55]

(Varney et al., 2017) tested the coupling of tapering and blowing into the base effects to reduce the drag of a visually square geometry. Slots have been introduced in the upper side and roof trailing edges of a square back geometry to take air from the free stream and passively inject it into the base of the vehicle to effectively create a tapered body. This investigation has been conducted in the Loughborough University's Large Wind Tunnel with the  $\frac{1}{4}$  scale generic SUV model. The basic aerodynamic effect of a range of body tapers and straight slots have been assessed for  $0^\circ$  around z-axis. This includes force and pressure measurements for most configurations. The slots generate useful, but small, drag reductions with the best configurations giving reductions in drag coefficient  $C_d$  of approximately 0.01, whereas the best taper configurations reduce  $C_d$  by close to 0.035. The slots also have a tendency to modify the lift [52].

## **8 CONCLUSION**

For ground vehicles, the fuel consumption accounts for over 30% of CO<sub>2</sub> and other greenhouse gas (GHG) emissions. The aerodynamic drag of a road vehicle is responsible for a large part of the vehicle's fuel consumption and contributes up to 50% of the total vehicle fuel consumption at highway speeds. Reducing the aerodynamic drag offers an inexpensive solution to improve fuel efficiency and thus reduce GHG emissions.

The two main methods of controlling the wake flow of ground vehicles are passive control (vortex generator, underbody device, deflector, tail plate ...) which is based on

the installation of a device on the car to modify the vortices, and active control (steady blowing, pulsed jets, suction, fluid oscillators...) which modify the wake of a car by using an additional energy. There are also approaches that use coupling between different methods, including passive and active, to further reduce the aerodynamic drag of the vehicle and thereby increase the potential for fuel economy.

Among flow control methods developed by researchers, there are those already industrialized and marketed, while others still in the process of improvement because of the design and habitability constraints.

According to the type of vehicle, and the industrialized aerodynamic arrangement methods, passive control can decrease the drag by 3.87% to 28%. Moreover, active methods allow drag reduction between 5% and 22%. In addition, coupling methods can reduce the aerodynamic drag up to 50%. Due to its wide range of applications, passive flow control is preferable. The advantages of this approach is that it requires no energy expenditure, no input from the user and is less expensive than an active technique.

## 9 SUMMARY

The classification of flow control methods reviewed in this paper, and others that exist in the literature, the models used, the parameters tested and the performance of each method to reduce aerodynamic drag were reported as a summary in the following tables:

PASSIVE CONTROL METHODS							
Control type	Author	Date	Experimental study	Numerical study	Passenger car model	Parameters	$C_d$ [%]
Tail plate	Sharma, R. B.	2013		* <u>Solver</u> : ANSYS 14.0 Fluent * <u>Turbulent model</u> : k- $\epsilon$	* <u>Model</u> : Passenger car * <u>Scale</u> : 1:1	* <u>Inlet velocity</u> : $U_o=22$ m/s * <u>Reynolds number</u> : $Re=1.3 \times 10^6$	3.87%
Non-smooth surface	Yiping, W.	2016		* <u>Solver</u> : ANSYS	* <u>Model</u> : Ahmed body * <u>Scale</u> : 1:1	* <u>Optimization model</u> : Kriging surrogate * <u>Inlet velocity</u> : $U_o=40$ m/s for $Re=2.78 \times 10^6$	5.20%
Rear screen & fairing	Rohatgi, U. S.	2012	* <u>Wind tunnel</u> : (TAD-2 of the National Aviation University of Ukraine (NAU))		* <u>Model</u> : SUV General Motor * <u>Scale</u> : Small (length 1710 mm)	* <u>Inlet velocity</u> : $U_o < 42$ m/s * <u>Turbulence intensity</u> : 0,9% * <u>Length of working section</u> : 5.5 m	6.5%-26%
Underbody devices	Junho, H.	2017		* <u>Solver</u> : Fluent * <u>Turbulent model</u> : k- $\epsilon$	* <u>Model</u> : YF-Sonata from Hyundai Motor Company (HMC) * <u>Scale</u> : 1:1	* <u>Inlet velocity</u> : $U_o=33.33$ m/s * <u>Reynolds number</u> : $Re=1.025 \times 10^7$	8.40%
Deflector	Fourrié, G.	2010	* <u>Wind tunnel</u> : Subsonic (TEMPO) at the University of Valenciennes * <u>Measurements</u> : Standard and stereoscopic PIV, Kiel pressure probes and surface flow visualization		* <u>Model</u> : Ahmed body * <u>Rear sland angle</u> : $25^\circ$ * <u>Scale</u> : 1:1	* <u>Inlet velocity</u> : $U_o=16$ m/s and 40 m/s * <u>Reynolds number</u> : $Re=3.1 \times 10^5$ to $Re=7.7 \times 10^5$	9%
	Hanfeng, W.	2015	* <u>Wind tunnel</u> : Central South University Cobra probe (Turbulent Flow Instrumentation Ltd; TFI) * <u>Measurements</u> : Pressure scanner Oil film flow visualization technique		* <u>Model</u> : Ahmed body * <u>Rear sland angle</u> : $25^\circ$ * <u>Scale</u> : 1:2	* <u>Inlet velocity</u> : $U_o=25$ m/s * <u>Reynolds number</u> : $Re=8.7 \times 10^5$ * SEM (side-edge-mounted): $H_d/l=2\%$ ; 3% * TEM (top-edge-mounted): $W_d/l=1\%$ ; 2%; 3%	3.9%-11.8%
	Raina, A.	2017		* <u>Grid generator</u> : GAMBIT * <u>Solver</u> : Fluent * <u>Turbulent model</u> : SST k- $\omega$	* <u>Model</u> : Ahmed body * <u>Rear sland angle</u> : $25^\circ$ * <u>Scale</u> : 1:4	* <u>Deflector angle</u> : $\theta=5^\circ$ * <u>Inlet velocity</u> : $U_o=40$ m/s * <u>Reynolds number</u> : $Re=7.7 \times 10^5$	7%
	Raina, A.	2018		* <u>Grid generator</u> : GAMBIT * <u>Solver</u> : Fluent * <u>Turbulent model</u> : k- $\omega$	* <u>Model</u> : Ahmed body * <u>Rear sland angle</u> : $25^\circ$ * <u>Scale</u> : 1:4	* <u>Deflector angle</u> : $\theta=5^\circ$ * <u>Inlet velocity</u> : $U_o=80$ m/s	13.34%
Vortex generator	Aider, J.L.	2010	* <u>Wind tunnel</u> : PSA Peugeot- Citroen in-house open wind tunnel * <u>Measurements</u> : Aerodynamic balance, PIV & boundary-layer hot-wire probe		* <u>Model</u> : Ahmed body * <u>Rear sland rounded</u> * <u>Scale</u> : 1:1	* <u>Inlet velocity</u> : $U_o=20$ m/s to 40 m/s * <u>Reynolds number</u> : $Re=1.2 \times 10^6$ to $2.4 \times 10^6$ * Yaw angle = $0^\circ$ * Turbulence intensity = 1.3%	12%

	Arya, S.	2017		* <u>CAD</u> : CATIA * <u>Solver</u> : ANSYS CFX * <u>Equations</u> : DES	* <u>Model</u> : Passenger car * <u>Scale</u> : 1:1	* <u>Inlet velocity</u> : $U_o=30$ m/s * <u>Reynolds number</u> : $Re=2.56 \times 10^5$	8.70%
Streaks	Pujals, G.	2010	* <u>Wind tunnel</u> : PSA type Eiffel with a rectangular cross section of 2.1 m high, 5.2 m wide and 6 m long		* <u>Model</u> : Ahmed body * <u>Rear sland angle</u> : $25^\circ$ * <u>Scale</u> : 1:1	* <u>Inlet velocity</u> : $U_o=5$ up to 55 m/s * <u>Reynolds number</u> : $Re=1.35 \times 10^6$	10%
Jet Boat Tail	Hirst, T.	2015	* <u>Wind tunnel</u> : University of Miami * <u>Measurements</u> : PIV	* <u>Equations</u> : LES	* <u>Model</u> : Rectangular prism bluff body 230×150×200mm	* <u>Inlet velocity</u> : $U_o=10$ m/s and 30 m/s * <u>Reynolds number</u> : $Re=0.85 \times 10^5$ and $Re=2.56 \times 10^5$	15%
Lateral Guide Vanes	Wahba, E.	2012		* <u>Solver</u> : ANSYS CFX * <u>Equations</u> : RANS * <u>Turbulent model</u> : k- $\epsilon$ ; SST k- $\omega$	* <u>Model</u> : Simplified SUV * <u>Scale</u> : 1:1	* <u>Inlet velocity</u> : $U_o=33.33$ m/s * <u>Reynolds number</u> : $Re=1.025 \times 10^7$	18%
Underbody diffuser	Kang, S. O.	2012		* <u>Optimisation model</u> : VMF (Vehicle Modeling Function) * <u>Solver</u> : ANSYS Fluent * <u>Equations</u> : DES; LES; RANS	* <u>Model</u> : Passenger car type notchback * <u>Scale</u> : 1:1	* <u>Inlet velocity</u> : $U_o=19.44$ m/s to 44.44 m/s * <u>Reynolds number</u> : $Re > 8 \times 10^6$ * <u>Diffuser length</u> : 450 mm	4%
	Marklund, J.	2013	* <u>Wind tunnel</u> : Saab Climatic	* <u>Solver</u> : Fluent 14.0 * <u>Equations</u> : RANS * <u>Turbulent model</u> : k- $\epsilon$	* <u>Model</u> : Saab 9-3 Sedan * <u>Scale</u> : 1:1	* <u>Inlet velocity</u> : $U_o=11.1$ m/s to 55.6 m/s	10%
	Mazyan, W. I.	2013		* <u>Solver</u> : ANSYS V11.0 * <u>Equations</u> : LES; RANS * <u>Turbulent model</u> : SST; RNG; k- $\epsilon$	* <u>Model</u> : Ahmed body * <u>Rear sland angle</u> : $30^\circ$ * <u>Scale</u> : 1:1 * <u>Type</u> : SUV Hammer	* <u>Inlet velocity</u> : $U_o=24.4$ m/s * <u>Generated meshes volume</u> : 2 million	4.2%-10%
	Huminic, A.	2017		* <u>Solver</u> : ANSYS CFX	* <u>Model</u> : Ahmed body * <u>Rear sland angle</u> : $35^\circ$ * <u>Scale</u> : 1:4	* <u>Inlet velocity</u> : $U_o=25$ m/s * <u>Reynolds number</u> : $Re=1.7 \times 10^6$ * $\alpha_d=5^\circ$ , $(l_d/l)=0.2$ * $\alpha_d=3^\circ$ , $(l_d/l)=0.4$	5.8%
Vertical splitter plate	Gilliéron, P.	2010	* <u>Wind tunnel</u> : Prandtl-type closed * <u>Measurements</u> : Three-component aerodynamic balance		* <u>Model</u> : Ahmed body * <u>Rear sland angle</u> : $90^\circ$ and $25^\circ$ * <u>Scale</u> : 3:4	* <u>Inlet velocity</u> : $U_o=20$ m/s and $U_o=30$ m/s * <u>Reynolds number</u> : $Re=1.09 \times 10^6$ - $Re=1.69 \times 10^6$	28%

ACTIVE CONTROL METHODS							
Control type	Author	Date	Experimental study	Numerical study	Passenger car model	Parameters	C <sub>d</sub> [%]
Fluidic oscillator	Metka, M.	2015	* <u>Wind tunnel</u> : 3feet×5feet subsonic wind tunnel at the Ohio State Aerospace Research Center. * <u>Measurements</u> : PIV and pressure taps		* <u>Model</u> : Ahmed body * <u>Rear sland angle</u> : 25° * <u>Scale</u> : 1:4	* <u>Inlet velocity</u> : U <sub>0</sub> =22.5 m/s * <u>Reynolds number</u> : Re=1.4 ×10 <sup>6</sup>	7%
Synthetic jets	Kourta, A.	2013	* <u>Wind tunnel</u> : Closed-loop wind tunnel located at the PRISME laboratory, University of Orleans. * <u>Measurements</u> : Static pressure, wall visualization and PIV		* <u>Model</u> : Ahmed body * <u>Rear sland angle</u> : 25° * <u>Scale</u> : 0.7	* <u>Inlet velocity</u> : U <sub>0</sub> =25 m/s and U <sub>0</sub> =40 m/s * <u>Reynolds number</u> : Re=1.2×10 <sup>6</sup> & Re=1.9×10 <sup>6</sup> * Actuator Lumped Element Modeling (LEM) placed at 2mm before the top of the rear window	6.5%-8.5%
Suction	Harinaldi, B.	2012	* <u>Wind tunnel</u>	* <u>Solver</u> : Fluent 6.3 * <u>Turbulent model</u> : k-ε	* <u>Model</u> : Ahmed Body * <u>Rear sland angle</u> : 35° * <u>Scale</u> : 1:4 * <u>Type</u> : Van Model (modified/Reversed)	* <u>Inlet velocity</u> : U <sub>0</sub> =13.9 m/s * <u>Reynolds number</u> : Re=2.48×10 <sup>5</sup> * Suction Velocity = 1 m/s	13.86%-16.32%
	Ait Moussa, A.	2014		* <u>CAD</u> : Solidworks 2013 * <u>Solver</u> : ANSYS * <u>Programming</u> : VBA	* <u>Model</u> : Sport Utility Vehicle (SUV) without side mirrors * <u>Scale</u> : 1:10	* <u>Inlet velocity</u> : U <sub>0</sub> =30 m/s * <u>Reynolds number</u> : Re=7.95×10 <sup>5</sup> * <u>Optimization method</u> : Taguchi	9%
A trip of pulse jets	Bideaux, E.	2011	* <u>Wind tunnel</u> : Malavard subsonic wind tunnel of the PRISME Institute in Orleans		* <u>Model</u> : Ahmed body * <u>Rear sland angle</u> : 35° * <u>Scale</u> : 0.7	* <u>Inlet velocity</u> : U <sub>0</sub> =30 m/s * <u>Reynolds number</u> : Re=1.4×10 <sup>6</sup> * Pulsed frequency : F=500 Hz * <u>Momentum coefficient</u> : C <sub>μ</sub> =2.75×10 <sup>-3</sup>	20%
	Joseph, P.	2013	* <u>Wind tunnel</u> : S4 full-scale automotive wind tunnel at the Institut Aero Technique (IAT)		* <u>Model</u> : Ahmed body * <u>Rear sland angle</u> : 25° * <u>Scale</u> : 1:1	* <u>Inlet velocity</u> : U <sub>0</sub> =30 m/s * <u>Reynolds number</u> : Re=1.4×10 <sup>6</sup>	10%
	Barros, D.	2014	* <u>Wind tunnel</u> : PSA-Peugeot Citroën wind tunnel * <u>Measurements</u> : Particle Image Velocimetry (PIV) and Hot Wire Anemometry (HWA)		* <u>Model</u> : Ahmed body * <u>Type</u> : Square-back. * <u>Scale</u> : 0.8	* <u>Inlet velocity</u> : U <sub>0</sub> =15 m/s * <u>Reynolds number</u> : Re=3×10 <sup>5</sup>	7%
	Barros, D.	2016	* <u>Wind tunnel</u> : type Subsonic * <u>Measurements</u> : PIV and Hot-Wire Anemometry (HWA).		* <u>Model</u> : Three-dimensional blunt body 893×350×297mm * <u>Rear sland angle</u> : 90°	* <u>Inlet velocity</u> : U <sub>0</sub> =15 m/s * <u>Reynolds number</u> : Re=3×10 <sup>5</sup> * <u>Turbulence intensity</u> : 0.5%	20%

	Ruiying, L.	2017	* <u>Wind tunnel</u> : type Closed-loop		* <u>Model</u> : Ahmed body * <u>Rear sland</u> : blunt-edged	* <u>Inlet velocity</u> : $U_o=15$ m/s * <u>Reynolds number</u> : $Re=3 \times 10^5$ * <u>Pressure sensors number</u> : 16	22%
Steady blowing microjets	Wassen, E.	2010		* <u>Solver</u> : SGI Attix supercomputer at the North German Cooperation for High-Performance Computing (HLRN) * <u>Equation</u> : LES	* <u>Model</u> : Ahmed Body * <u>Rear sland angle</u> : $90^\circ$ * <u>Scale</u> : 1:1	* <u>Inlet velocity</u> : $U_o=15$ m/s * <u>Reynolds number</u> : $Re=5 \times 10^5$ * <u>Blowing angle</u> : $\theta = 45^\circ$ * <u>Blowing velocity</u> : $V_{blow}=1.25 U_o$	11.10%
	Aubrun, S.	2011	* <u>Wind tunnel</u> : Malavard wind tunnel of the PRISME Institute, University of Orleans * <u>Measurements</u> : PIV and wall pressure measurements and skin friction visualizations		* <u>Model</u> : Ahmed body * <u>Rear sland angle</u> : $25^\circ$ * <u>Scale</u> : 0.7	* <u>Inlet velocity</u> : $U_o=40$ m/s * <u>Reynolds number</u> : $Re=1.95 \times 10^6$	9-14%
	Harinaldi, B.	2013	* <u>Wind tunnel</u>	* <u>Solver</u> : Fluent 6.3 * <u>Grid generator</u> : GAMBIT 2.4 * <u>Generated meshes volume</u> : 1.7 million * <u>Turbulent model</u> : k- $\epsilon$	* <u>Model</u> : Ahmed Body * <u>Rear sland angle</u> : $35^\circ$ * <u>Scale</u> : 1:4 * <u>Type</u> : Van Model (modified/Reversed)	* <u>Inlet velocity</u> : $U_o=13.9$ m/s-19.44 m/s * <u>Reynolds number</u> : $Re=2.48 \times 10^5$ * <u>Blowing velocity</u> : $V_{blow}=0.5$ m/s	11.11%-13.92%
	Heinemann, T.	2014	* <u>Wind tunnel</u> : Friedrich Alexander University in Erlangen-Nuremberg (FAU) and the Technische Universität München (TUM) * <u>Measurements</u> : Laser Doppler Anemometry, surface pressure measurements, surface oil flow visualization		* <u>Model</u> : Commercial automobile * <u>Scale</u> : 1:4	* <u>Inlet velocity</u> : $U_o=30$ m/s * <u>Reynolds number</u> : $Re=1.2 \times 10^6$	5%
	McNally, J.W.	2015	* <u>Wind tunnel</u> : FCAA Plow speed	* <u>Solver</u> : CharLES from Cascade Technologies, Inc.	* <u>Model</u> : Honda Simplified Body (HSB) * <u>Type</u> : Flat-back with rounded front and rear edges	* <u>Inlet velocity</u> : $U_o=28$ m/s * <u>Reynolds number</u> : $Re=9.7 \times 10^5$	13%
Plasma actuator	Shadmani, S.	2018	* <u>Wind tunnel</u> : the open circuit wind tunnel at K. N. Toosi University (Iran)		* <u>Model</u> : Ahmed body * <u>Rear sland angle</u> : $25^\circ$ * <u>Scale</u> : 0.64	* <u>Inlet velocity</u> : $U_o=10$ m/s * <u>Reynolds number</u> : $Re=4.5 \times 10^5$	3.65%

COUPLING OF CONTROL METHODS

Control type	Author	Date	Experimental study	Numerical study	Passenger car model	Parameters	$C_d$ [%]
Blowing, pulsed jets and porous layers	Bruneau, C. H.	2010		* <u>Simulation method</u> : Cartesian grids	* <u>Model</u> : Ahmed body * <u>Rear sland angle</u> : 90° * <u>Scale</u> : 1:1	* <u>Reynolds number</u> : $Re=0.3 \times 10^5$ * <u>Momentum coefficient</u> : $C_\mu=4 \times 10^{-3}$	30%
Sucking and blowing jets	Harinaldi, B.	2011		* <u>Solver</u> : Fluent 6.3 * <u>Turbulent model</u> : k-ε	* <u>Model</u> : Ahmed Body * <u>Rear sland angle</u> : 35° * <u>Scale</u> : 1:4 * <u>Type</u> : Van Model (modified/Reversed)	* <u>Inlet velocity</u> : $U_0=1$ m/s, 5 m/s, 10 m/s, 15 m/s * <u>Reynolds number</u> : $Re=2.98 \times 10^5$	14.38%-15.83%
	Jahanmiri. M.	2011	* <u>Wind tunnel</u> : Subsonic closed circuit with a closed test section		* <u>Model</u> : Ahmed body * <u>Rear sland angle</u> : 35° * <u>Scale</u> : 1:1	* <u>Control flow rates</u> : $>0.0035$ m <sup>3</sup> /s * <u>Reynolds number</u> : $Re=2.8 \times 10^6$	29.50%
Steady blowing with base cavity	Khalighi, B.	2012	* <u>Wind tunnel</u> : Scale small GM R&D Basic Research	* <u>Equation</u> : URANS * <u>Turbulent model</u> : $v^2$ -f	* <u>Model</u> : Square-back car * <u>Scale</u> : 1:1	* <u>Inlet velocity</u> : $U_0=50$ m/s * <u>Reynolds number</u> : $Re=1.25 \times 10^6$	18%-50%
Tapering and blowing into the base	Varney, M	2017	* <u>Wind tunnel</u> : Loughborough University Large wind tunnel with an open circuit and closed throat		* <u>Model</u> : SUV * <u>Scale</u> : 1:4	* <u>Straight slots</u> : 0° yaw	3.50%

## REFERENCES

- [1] Eulalie, Y., Étude aérodynamique et contrôle de la traînée sur un corps d’Ahmed culot droit, PhD Thesis University of Bordeaux, France, 2014.
- [2] Blocken, B., Toparlar, Y., “A following car influences cyclist drag: CFD simulations and wind tunnel measurements”, Journal of Wind Engineering and Industrial Aerodynamics, vol. 145, pp. 178-186, 2015.
- [3] Hucho, W.H., Sovran, G., “Aerodynamics of road vehicles”, Annual Review of Fluid Mechanics, vol. 25, no. 1, pp. 485-537, 1993.
- [4] Sudin, M.N., Abdullah, M.N., Shamsuddin, S.A., Ramli, F.R., Tahir, M.M., “Review of research on vehicles aerodynamic drag reduction methods”, International Journal of Mechanical & Mechatronics Engineering IJMME-IJENS, vol. 14, no. 02, pp. 35-47, 2014.
- [5] Eulalie, Y., Gilotte, P., Mortazavi, I., “Numerical study of flow control strategies for a simplified square background vehicle”, Fluid Dyn. Res., vol. 49, pp. 1-25, 2017.
- [6] Onorato, M., Costelli, A.F., Garonne, A., “Drag measurement through wake analysis”, SAE International Congress and Exposition, No. SP6569, pp. 85-93, Detroit, 1984.
- [7] Guilmineau, E., “Computational study of flow around a simplified car body”, Journal of Wind Engineering and Industrial Aerodynamics, vol. 96, no. 6-7, pp. 1207–1217, 2008.
- [8] Bello-Millan, F.J., Makela, T., Parras, L., Del Pino, C., Ferrera, C., “Experimental study on Ahmed's body drag coefficient for different yaw angles”, Journal of Wind Engineering and Industrial Aerodynamics, vol. 157, pp. 140–144, 2016.
- [9] Meile, W., Ladinek, T., Brenn, G., Reppenhagen, A., Fuchs, A. “Non-symmetric bi-stable flow around the Ahmed body”, International Journal of Heat and Fluid Flow, vol. 57, pp. 34-47, 2016.
- [10] Rao, A., Minelli, G., Basara, B., Krajnovi, S., “On the two flow states in the wake of a hatchback Ahmed body”, Journal of Wind Engineering and Industrial Aerodynamics, vol. 173, pp. 262–278, 2018.
- [11] Ahmed, S.R., Ramm, G., Faltin, G., “Some salient features of the time averaged ground vehicle wake”, SAE Technical Paper Series 840300, 1984.
- [12] Kourta, A., Leclerc, C., “Characterization of synthetic jet actuation with application to Ahmed body wake”, Sensors and Actuators A: Physical, vol. 192, pp. 13– 26, 2013.

- [13] Bideaux, E., Bobillier, P., Fournier, E., Gilliéron, P., Hajem, M., Champagne, J. Y., Kourta, A., "Drag reduction by pulsed jets on strongly unstructured wake: towards the square back control", *International Journal of Aerodynamics*, vol. 1, no. 3, pp. 282-298, 2011.
- [14] Joseph, P., Amandolese, X., Edouard, C., Aider, J.L., "Flow control using MEMS pulsed micro-jets on the Ahmed body", *Exp. Fluids*, vol. 54, no. 1, pp. 1–12, 2013.
- [15] Barros, D., Ruiz, T., Boree, J., Noack, B.R., "Control of a three-dimensional blunt body wake using low and high frequency pulsed jets", *International Journal of Flow Control*, vol. 6, no. 1, pp. 61–74, 2014.
- [16] Barros, D., Borée, J., Noack, B.R., Spohn, A., Ruiz, T., "Bluff body drag manipulation using pulsed jets and Coanda effect", *Journal of Fluid Mechanics*, vol. 805, pp. 422-459, 2016.
- [17] Edwige, S., Eulalie, Y., Gilotte, P., Mortazavi, I., "Wake flow analysis and control on a 47° slant angle Ahmed body", *International Journal of Numerical Methods for Heat & Fluid Flow*, pp. 1-11, 2018.
- [18] Harinaldi, Budiarmo, Warjito, Kosasih, E.A., Tarakka, R., Simanungkalit, S.P., "Modification of flow structure over a van model by suction flow control to reduce aerodynamics drag", *Makara Seri Teknologi*, vol. 16, no. 1, pp. 15-21, 2012.
- [19] Ait Moussa, A., Yadav, R., Fischer, J., "Aerodynamic drag reduction for a Generic Sport Utility Vehicle using rear suction", *Journal of Engineering Research and Applications*, vol. 4, no. 8, pp. 101-107, 2014.
- [20] Wassen, E., Thiele, F., Simulation of active separation control on a generic vehicle, In at: 5th AIAA Flow Control Conference, Chicago, USA, 2010.
- [21] Aubrun, S., McNally, J., Alvi, F., Kourta, A., "Separation flow control on a generic ground vehicle using steady microjet arrays", *Experiments in fluids*, vol. 51, no. 5, pp. 1177-1187, 2011.
- [22] Harinaldi, Budiarmo, Tarakka, R., Simanungkalit, S.P., "Effect of active control by blowing to aerodynamic drag of bluff body van model", *International Journal of Fluid Mechanics Research*, vol. 40, no. 4, pp. 312-323, 2013.
- [23] Heinemann, T., Springer, M., Lienhart, H., Kniesburgs, S., Becker, S., "Active flow control on a 1:4 car model", *Exp. Fluids*, vol. 55, no. 1738, pp. 1-11, 2014.
- [24] Metka, M., Gregory, J.W., "Drag reduction on the 25-deg Ahmed model using fluidic oscillators", *J. Fluids Eng.*, vol. 137 (051108), 1-8. 2015.
- [25] Gilliéron, P., Kourta, A., "Aerodynamic drag reduction by vertical splitter plates", *Experiments in Fluids*, vol. 48, no. 1, pp. 1-16, 2010.
- [26] Beaudoin, J.F., Aider, J.L., "Drag and lift reduction of a 3D bluff body using flaps", *Experiments in Fluids*, vol. 44, pp. 491–501, 2008.
- [27] Altaf, A., Omar, A.A., Asrar, W., "Review of passive drag reduction techniques for bluff road vehicles", *IJUM Engineering Journal*, vol. 15, no. 1, pp. 61-69, 2014.
- [28] Omar, A.A., Asrar, W., "Passive drag reduction of square back road vehicles", *Journal of Wind Engineering and Industrial Aerodynamics*, vol. 134, pp. 30–43, 2014.
- [29] Aider, J.L., Beaudoin, J.F., Wesfreid, J.E., "Drag and lift reduction of a 3D bluff body using vortex generators", *Experiments in Fluids*, vol. 48, no. 5, pp. 771-789, 2010.
- [30] Kim, I., Chen, H., "Reduction of aerodynamic forces on a minivan by a pair of vortex generators of a pocket type", *International Journal of Vehicle Design*, vol. 53, no. 4, pp. 300-316, 2010.
- [31] Rohatgi, U.S. Methods of reducing vehicle aerodynamic drag, ASME 2012, Summer Heat Transfer Conference, Puerto Rico, USA, July 8-12, 2012.
- [32] Dubey, A., Chheniya, S., Jadhav, A., "Effect of vortex generators on aerodynamics of a car: CFD analysis", *International Journal of Innovations in Engineering and Technology (IJJET)*, vol. 2, no. 1, pp. 137-144, 2013.
- [33] Arya, S., Goud, P., Mathur, S., Sharma, V., Tripathi, S., Shukla, V., "A review on "Reduction of drag force using ADD-ON Devices", *International Research Journal of Engineering and Technology (IRJET)*, vol.3, no. 11, pp. 985-994, 2017.
- [34] Thacker, A., Aubrun, S., Leroy, A., Devinant, P., "Effects of suppressing the 3D separation on the rear slant on the flow structures around an Ahmed body", *Journal of Wind Engineering and Industrial Aerodynamics*, 107–108, pp. 237–243, 2012.
- [35] Fourrié, G., Keirsbulck, L., Labraga, L., Gilliéron, P., "Bluff-body drag reduction using deflector", *Experiments in Fluids*, vol. 50, no. 2, pp. 385-395, 2011.
- [36] Raina, A., Harmain, G.A., Mir-Irfan, U.H., "Numerical investigation of flow around a 3D bluff body using deflector plate", *International Journal of Mechanical Sciences*, pp. 1-25, 2017.
- [37] Raina, A., Khajuria, A., "Flow control around a 3d-bluff body using passive device", *International Journal of Science And Engineering*, vol. 4, no. 1, pp. 8-13, 2018.
- [38] Yiping, W., Cheng, W., Gangfeng, T., Yadong, D., "Reduction in the aerodynamic drag around a generic vehicle by using a non-smooth surface", *Proceedings of the Institution of Mechanical Engineers, Part D: Journal of Automobile Engineer*, pp. 1-15, 2016.

- [39] Junho, C., Tae-Kyung, K., Kyu-Hong, K., Kwanjung, Y., "Comparative investigation on the aerodynamic effects of combined use of underbody drag reduction devices applied to real Sedan", *International Journal of Automotive Technology*, vol. 18, no. 6, pp. 959-971, 2017.
- [40] Pujals, G., Depardon, S., Cossu, C., "Drag reduction of a 3D bluff body using coherent streamwise streaks", *Experiments in Fluids*, vol. 49, no. 5, pp. 1085-1094, 2010.
- [41] Hirst, T., Li, C., Yang, Y., Brands, E., Zha, G., "Bluff body drag reduction using passive flow control of Jet Boat Tail", *SAE Int. J. Commer. Veh.*, vol. 8, no. 2, pp. 713-721, 2015.
- [42] Howell, J., Sims-Williams, D., Sprot, A., Hamlin, F., Dominy, R., "Bluff body drag reduction with ventilated base cavities", *SAE Int. J. Passenger Cars - Mech. Syst.*, vol. 5, no. 1, pp. 152-160, 2012.
- [43] Khalighi, B., Balkanyi, S.R., Bernal, L.P., "Experimental investigation of aerodynamic flow over a bluff body in ground proximity with drag reduction devices", *Int. J. Aerodynamics*, pp. 3, no. 4, pp. 217-233, 2013.
- [44] Wahba, E., Al-Marzooqi, H., Shaath, M., Shahin, M., El-Dhmarshawy, T., "Aerodynamic drag reduction for ground vehicles using lateral guide vanes", *CFD Letters*, vol. 4, no. 2, pp. 68-79, 2012.
- [45] Kang, S.O., Jun, S.O., Park, H.I., Song, K.S., Kee, J.D., Kim, K.H., Lee, D.H., "Actively translating a rear diffuser device for the aerodynamic drag reduction of a passenger car", *International Journal of Automotive Technology*, vol. 13, no. 4, pp. 583-592, 2012.
- [46] Marklund, J., Lofdahl, L., Danielsson, H., Olsson, G., "Performance of an automotive under-body diffuser applied to a sedan and a wagon vehicle", *SAE Inter. Journal of Passenger Cars-Mechanical Systems*, vol. 6, no. 1, pp. 293-307, 2013.
- [47] Mazyan, W.I., Numerical simulations of drag-reducing devices for ground vehicles, Doctoral dissertation, American University, 2013.
- [48] Humnic, A., Humnic, G., "Aerodynamic study of a generic car model with wheels and underbody diffuser", *International Journal of Automotive Technology*, vol. 18, no. 3, pp. 397-404, 2017.
- [49] Bruneau, C.H., Mortazavi, I., Gilliéron, P., "Passive control around the two-dimensional square back Ahmed Body using porous devices", *Journal of Fluids Engineering*, vol. 130 / 061101, pp. 1-12, 2008.
- [50] Sharma, R.B., Bansal, R., "CFD simulation for flow over passenger car using tail plates for aerodynamic drag reduction", *Journal of Mechanical and Civil Engineering (IOSR-JMCE)*, vol. 7, no. 5, pp. 28-35, 2013.
- [51] Bruneau, C.H., Creusé, E., Depeyras, D., Gilliéron, P., Mortazavi, I., "Coupling active and passive techniques to control the flow past the square back Ahmed body", *Computers & Fluids*, vol. 39, no. 10, 1875-1892, 2010.
- [52] Varney, M., Passmore, M., Gaylard, A., "The effect of passive base ventilation on the aerodynamic drag of a generic SUV vehicle", *SAE Int. J. Passeng. Cars - Mech. Syst.*, vol. 10, no. 1, pp. 345-357, 2017.
- [53] Harinaldi, B., Tarakka, R., Simanungkalit, S.P., "Computational analysis of active flow control to reduce aerodynamics drag on a van model", *International Journal of Mechanical & Mechatronics Engineering IJMME-IJENS*, vol. 11, no. 3, pp. 24-30, 2011.
- [54] Jahanmiri, M., Abbaspour, M., "Experimental investigation of drag reduction on Ahmed model using a combination of active flow control methods", *Inter. Journal of Engineering-Transactions A: Basics*, vol. 24, no. 4, pp. 403-410, 2011.
- [55] Khalighi, B., Chen, K.H., Iaccarino, G., "Unsteady aerodynamic flow investigation around a simplified square-back road vehicle with drag reduction devices", *Journal of Fluids Engineering*, vol. 134 (061101), pp. 1-16, 2012.
- [56] Kim, J.J., Lee, S., Kim, M., You, D., Lee, S.J., "Salient drag reduction of a heavy vehicle using modified cab-roof fairings", *Journal of Wind Engineering and Industrial Aerodynamics*, vol. 164, pp. 138-151, 2017.
- [57] Shim, H.S., Lee, Y.N., Kim, K.Y., "Optimization of bobsleigh bumper shape to reduce aerodynamic drag", *Journal of Wind Engineering and Industrial Aerodynamics*, vol. 164, pp. 108-118, 2017.
- [58] Hanfeng, W., Yu, Z., Chao, Z., Xuhui, H., "Aerodynamic drag reduction of an Ahmed body based on deflectors", *Journal of Wind Engineering and Industrial Aerodynamics*, vol. 148, pp. 34-44, 2015.
- [59] McNally, J., Fernandez, E., Robertson, G., Kumar, R., Taira, K., Alvi, F., Yamaguchi, Y., Murayama, K., "Drag reduction on a flat-back ground vehicle with active flow control", *Journal of Wind Engineering and Industrial Aerodynamics*, vol. 145, pp. 292-303, 2015.
- [60] Shadmani, S., Mousavi Nainiyan, S. M., Ghasemiasl, R., Mirzaei, M., Pouryoussefi, S.G., "Experimental study of flow control over an Ahmed body using plasma actuator", *Mechanics and Mechanical Engineering*, vol. 22, no. 1, pp. 239-251, 2018.
- [61] Ruiying, L., Bernd, R.N., Laurent, C., Jacques, B., Fabien, H., "Drag reduction of a car model by linear genetic programming control", *Exp. Fluids*, vol. 58, no. 103, pp. 1-20, 2017.